ACS Catalysis

Letter

pubs.acs.org/acscatalysis

Low-Overpotential Electroreduction of Carbon Monoxide Using Copper Nanowires

David Raciti,[†,¶] Liang Cao,[‡,§,¶] Kenneth J. T. Livi,[§] Paul F. Rottmann,[§,∥] Xin Tang,[⊥] Chenyang Li,[§] Zachary Hicks,[⊥] Kit H. Bowen,[⊥] Kevin J. Hemker,[∥] Tim Mueller,*[,§] and Chao Wang*[,†]

[†]Department of Chemical and Biomolecular Engineering, [‡]Department of Physics and Astronomy, [§]Department of Materials Science and Engineering, [∥]Department of Mechanical Engineering, and [⊥]Department of Chemistry, Johns Hopkins University, Baltimore, Maryland 21218, United States

Supporting Information

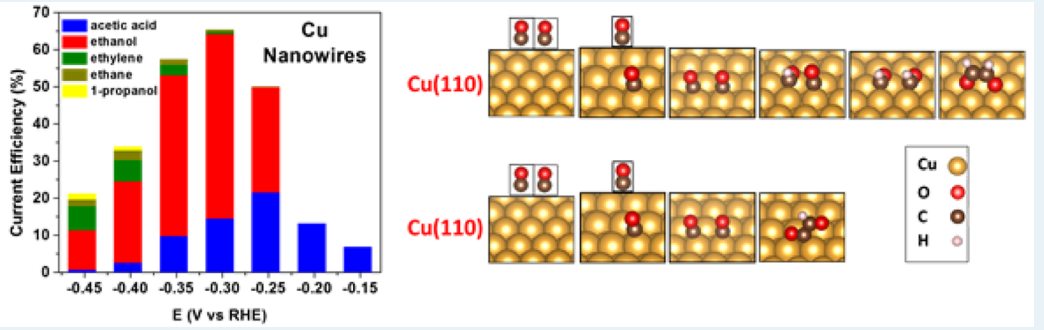

ABSTRACT: We report on Cu nanowires as highly active and selective catalysts for electroreduction of CO at low overpotentials. The Cu nanowires were synthesized by reducing pregrown CuO nanowires, with the surface structures tailored by tuning the reduction conditions for improved catalytic performance. The optimized Cu nanowires achieved 65% faradaic efficiency (FE) for CO reduction and 50% FE toward production of ethanol at potentials more positive than −0.5 V (versus reversible hydrogen electrode, RHE). Structural analyses and computational simulations suggest that the CO reduction activity may be associated with the coordinately unsaturated (110) surface sites on the Cu nanowires.

KEYWORDS: *electroreduction, carbon monoxide, copper nanowires*

Cu has been extensively studied as heterogeneous catalysts for CO hydrogenation in gas-phase reactions[1,2] and also as electrocatalysts for CO reduction in aqueous solutions.[3−6] The recent growth of interest in electrochemical CO_2 reduction, as a promising means for artificial carbon recycling and solar-fuel energy conversion,[7−9] has further stimulated the interest in CO reduction electrocatalysis, because CO is the intermediate for reduction of CO_2 to hydrocarbons and oxygenates.[10,11] Early studies of CO reduction on polycrystalline Cu surfaces reported the production of hydrocarbons such as methane and ethylene, but it requires large overpotentials (about −1.0 V versus RHE; the same reference electrode is used in the following discussion), and the efficiency is limited by the competing hydrogen evolution reaction (HER; with >40% faradaic efficiency (FE) toward H_2).[3,12] Investigations of Cu single crystals indicate that the CO reduction electrocatalysis is structure-sensitive,[5,13,14] with ethylene favorably produced on Cu(100) at low overpotentials via electron mediated CO−CO coupling.[15,16] Nanocrystalline Cu electrodes derived from cuprite were recently reported to be active for CO reduction at low overpotentials (i.e., more positive than −0.5 V), but selectively produce ethanol and acetate.[6] It is suggested that the active sites on these catalysts are associated with grain boundaries and bind to CO more strongly than low-index Cu facets.[17] Nevertheless, substantial challenges are still present in synthetic control and characterization of the surface structures for Cu-based nanocatalysts, which has limited the mechanistic understanding and design of more efficient electrocatalysts for CO (and CO_2) reduction.

Here we report on Cu nanowires as advanced electrocatalysts for electroreduction of CO at low overpotentials. Highly dense Cu nanowires were synthesized by thermal reduction of CuO nanowires using hydrogen, by modifying the method previously reported by our group.[18] Electrosorption of hydroxide (OH_{ad}) and temperature-programmed CO desorption (CO-TPD) were combined to probe the surface structures of these Cu nanowires. The obtained information was correlated to the catalytic activities and selectivities derived from electrochemical studies, on the basis of which density functional theory (DFT)[19] calculations were further performed to elucidate possible active sites and reaction pathways for low-overpotential CO reduction.

Received: April 5, 2017
Revised: May 24, 2017

DOI: 10.1021/acscatal.7b01124
ACS Catal. 2017, 7, 4467−4472

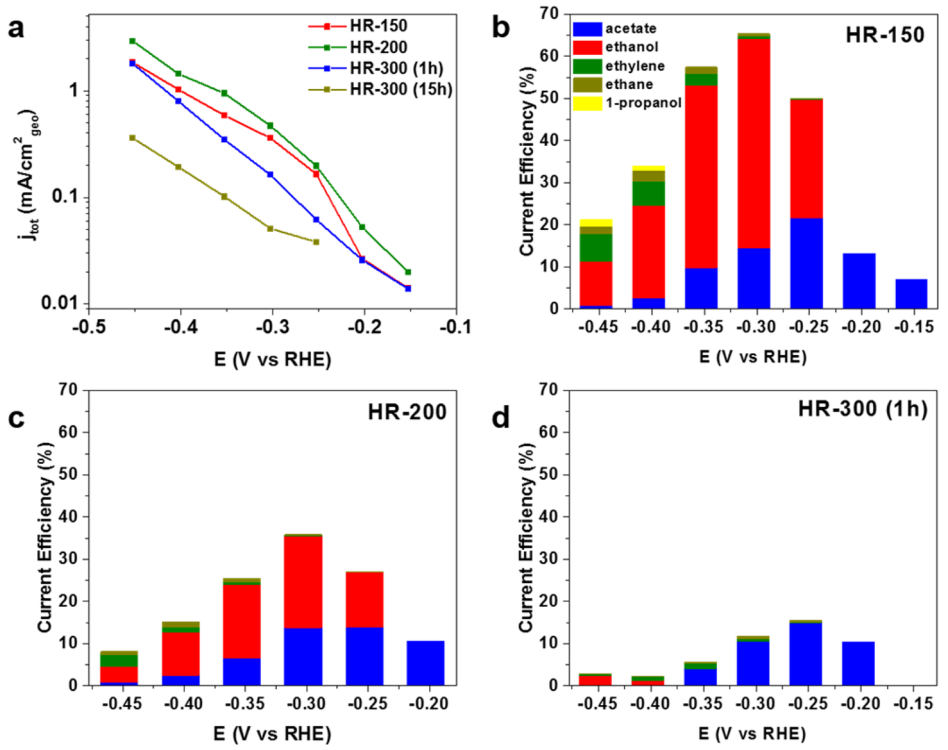

Figure 1. Electrocatalytic performance of the Cu nanowires for CO reduction. (a) Total current densities per geometric area of the electrode. (b–d) Product distributions depending on the electrode potential for the various types of Cu nanowires.

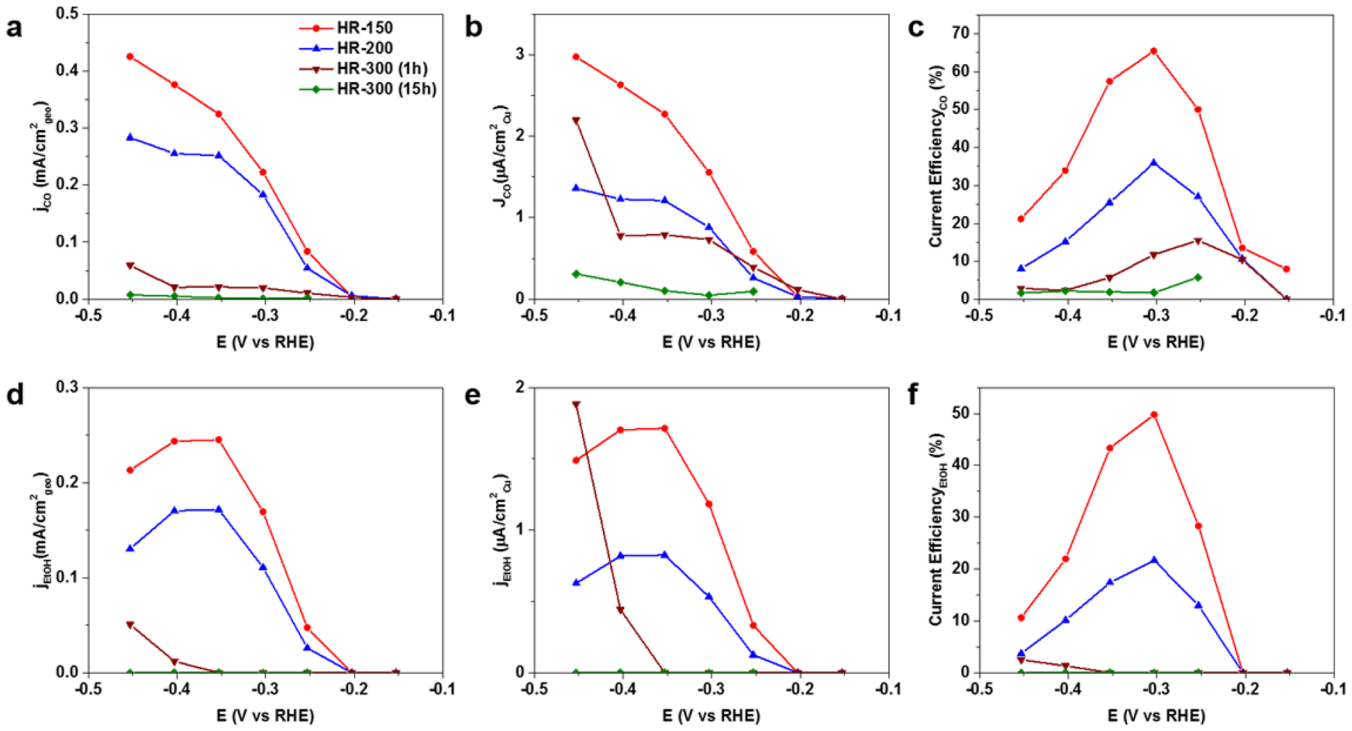

Figure 2. Comparison of catalytic performance for the various types of Cu nanowires. (a) Geometric current densities (per electrode area), (b) specific current densities (per ECSA), and (c) Faradaic efficiencies (FEs) for total CO reduction, namely, accounting for all the carbon-containing products. (d–f) Corresponding comparisons for the selectivity for reduction of CO to ethanol.

The Cu nanowires prepared by hydrogen reduction at 150, 200, and 300 °C are hereby denoted as HR-150, 200, 300, respectively (HR-300 (1 h) and HR-300 (15 h) for the nanowires annealed at 300 °C for 1 and 15 h, respectively) (Figure S1). Electrocatalytic studies for CO reduction were carried out in a gas-tight electrolysis cell containing 0.1 M KOH as the electrolyte. Gas- and liquid-phase products were analyzed by using gas chromatograph–mass spectrometry (GC-MS) and nuclear magnetic resonance (NMR) spectroscopy, respectively. The HR-200 nanowires generated the largest current density

DOI: 10.1021/acscatal.7b01124
ACS Catal. 2017, 7, 4467–4472

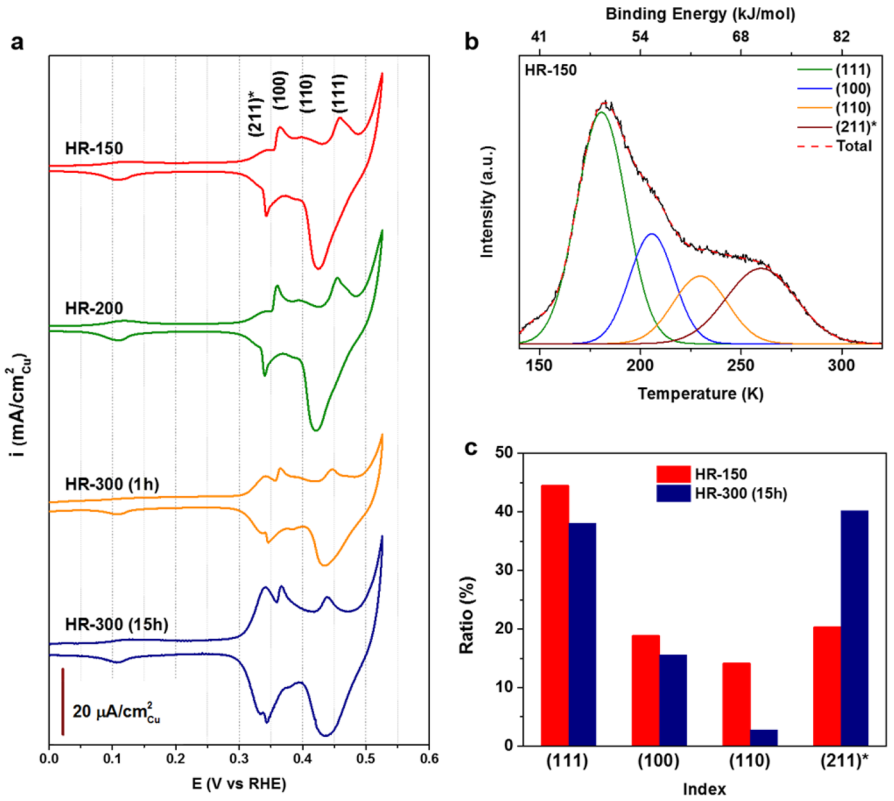

Figure 3. Surface structure analysis for the Cu nanowires. (a) Voltammograms collected in 1 M KOH showing the OH_{ad} peaks. (b) CO-TPD patterns collected for the HR-150 Cu nanowires. (c) Fractions of surface facets for the Cu nanowires derived from the CO-TPD patterns.

(per electrode area), achieving 0.48 mA/cm^2 at −0.3 V (Figure 1a), as compared to 0.36 mA/cm^2 for the HR-150 nanowires. The nanowires prepared at 300 °C gave much lower geometric current densities, at only 0.16 mA/cm^2 for the HR-300 (1 h) and 0.05 mA/cm^2 for the HR-300 (15 h) nanowires at the same potential. The trend of geometric current densities correlates well with the electrochemically active surface areas (ECSAs) estimated by electrochemical capacitance measurements, with the surface roughness factor found to decrease as the reduction temperature and time increase (Table S1). The current densities after taking the roughness factors into account are rather similar for the different types of Cu nanowires, except that the HR-300 (1 h) nanowires had a slightly higher value than the rest (Figure S4).

Throughout the studies, oxygenated C_2 hydrocarbons, ethanol, and acetate were found to be the major products of CO reduction. The various types of Cu nanowires exhibit consistent onset potentials at −0.15 ∼ − 0.20 V for CO reduction, whereas the HR-150 nanowires are the most selective catalyst at more negative potentials. In the latter case, production of acetate starts at −0.15 V with a FE of 7%, which increases to 21% at −0.25 V and then decreases as the potential goes more negative (Figure 1b). The production of ethanol appears at −0.25 V with an FE of 29% on the HR-150 nanowires and reaches the maximum FE of 50% at −0.30 V, which also drops as the potential goes more negative. Other C_2 products such as ethylene (up to 7%) and ethane (up to 2.3%), as well as a C_3 product, 1-propanol (up to 1.8%) are also produced at potentials more negative than −0.30 V. The total FE for CO reduction achieves 65% (at −0.30 V) for the HR-150 nanowires. The Cu nanowires prepared at higher temperatures have lower selectivities for CO reduction, with the total FE down to <37% for the HR-200 and <16% for the HR-300 (1 h) nanowires (Figure 1c,d). The HR-300 (1 h) nanowires produce some acetate (up to 15% FE at −0.25 V), whereas HR-300 (15 h) nanowires produce mostly hydrogen (>90% FE) (see supplemental Figure S9).

To better illustrate the differences in catalytic performance, we have compared the partial current densities for CO reduction (j_{CO}) and ethanol production (j_{EtOH}) and the corresponding FEs for the various types of Cu nanowires (Figure 2). Throughout the potential range examined here (−0.15 ∼ − 0.45 V), the geometric current densities for both CO reduction and ethanol production decrease as the preparation temperature increase (Figures 2a,d). The HR-150 nanowires have the highest geometric current densities, reaching 0.33 mA/cm$^2_{geo}$ for CO reduction and 0.25 mA/cm$^2_{geo}$ for ethanol production at −0.35 V. The HR-150 nanowires also possess the highest specific activity (namely, the current density with normalization of ECSA), generating 2.3 μA/cm$^2_{Cu}$ for CO reduction and 1.7 μA/cm$^2_{Cu}$ for ethanol production at −0.35 V (Figure 2b,e). For almost all of the nanowire catalysts the maximum FEs for CO reduction and ethanol production were reached at −0.30 V, with the HR-150 nanowires being the most selective (Figure 2c,f). It is noticed that the HR-150 nanowires outperformed at potentials more positive than −0.35 V as compared to the previously reported Cu electrodes derived from cuprite, in particular with a positive shift of the onset potential by ∼100 mV (Figure S10).

Previous reports on cuprite-derived Cu electrodes indicate that CO reduction activity is correlated to the density of crystal boundaries.[17,20] By examination of the Cu nanowires using scanning precession electron diffraction (SPED) analysis, we find that the density of grain boundaries decreases as the

DOI: 10.1021/acscatal.7b01124
ACS Catal. 2017, 7, 4467−4472

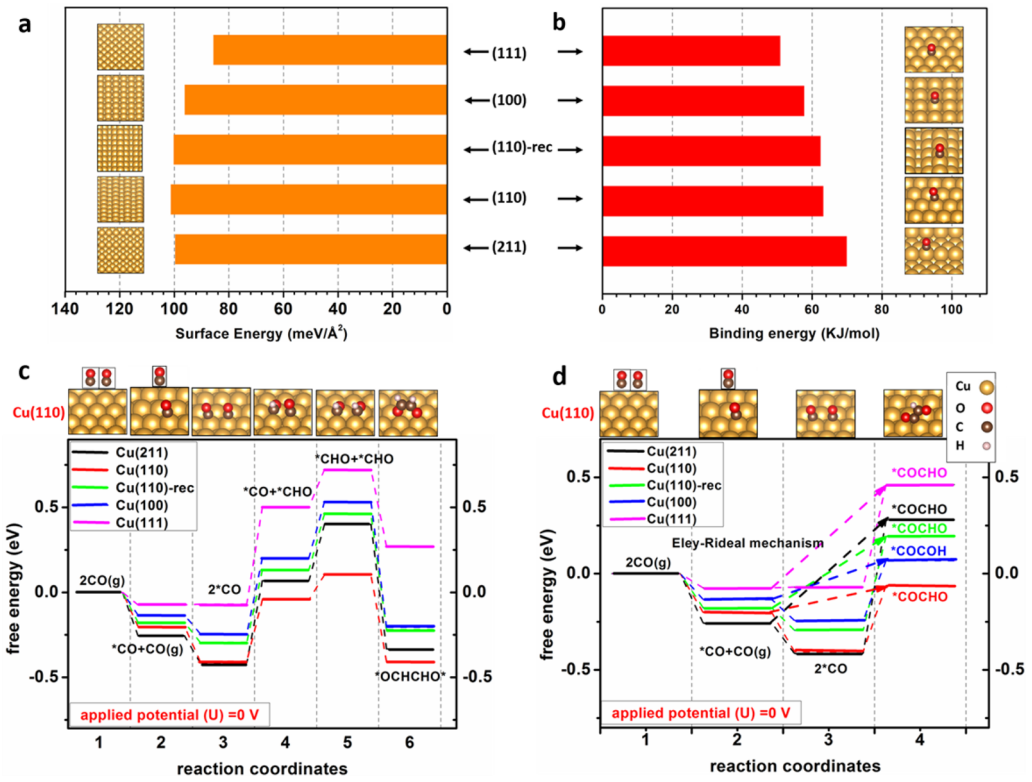

Figure 4. Simulation of the Cu surfaces for CO reduction based on DFT calculations. (a) Surface energies and (b) CO binding energies for different Cu facets; (c,d) Free-energy diagrams for CO reduction to C_2 products via (c) the CHO−CHO mechanism and (d) the CO−CO coupling mechanism. (110)-rec indicates a (110) surface with a missing-row reconstruction. The dashed arrows in (d) represent possible CO−CO coupling through an Eley−Rideal mechanism. The likely formation of $*OCCO^{\delta-}$ between steps 3 and 4 in (d) is not included for reasons discussed in the Supporting Information. The illustrations of the configurations of surface adsorbates are on the Cu(110) facet.

temperature of preparation increases (Figure S11), which is consistent with the previous observations on cuprite-derived Cu nanocrystals.[17,20] It is however difficult to derive surface structure information from such analyses for the polycrystalline Cu nanowires.[21,22] Direct imaging of the atomic structures on the surface of the Cu nanowires using high-resolution TEM (HRTEM), on the other side, was found to be challenging, partially due to surface oxidation after the nanowires were exposed to air.[18] To probe the surface structures of the Cu nanowires, we turned to electrochemical OH_{ad} and CO-TPD studies.

Various facets of Cu single crystals exhibit distinct OH_{ad} peaks at different potentials in voltammograms, allowing for the use of OH_{ad} to probe the surface structures of polycrystalline Cu electrodes.[23] The voltammograms measured for the Cu nanowires exhibit a series of reversible peaks in the potential region of 0.35−0.50 V, which can be assigned to the features of low-index facets of face-centered cubic (fcc) Cu (i.e., ∼0.36 V for (100), ∼0.43 V for (110), and ∼0.45 V for (111); Figure 3a). An additional shoulder peak was observed at ∼0.34 V, which was not reported before by the studies on extended surfaces. Because this peak appears at relatively low potentials, it is likely associated with more oxophilic surface sites than the low-index facets. We tentatively assign it to stepped surfaces such as (211) that have smaller coordination numbers. Based on the calculated OH adsorption energies (Table S10), this peak may also correspond to a reconstructed (110) surface. For simplicity, we denote it as (211)* in the following discussion. By comparing the voltammograms, it can be seen that the nanowires prepared at high temperatures have much more pronounced (211)* features, whereas the (110) peak almost diminishes (Figure 3a). The surface features shown in the voltammograms are largely preserved after the electrocatalytic studies, indicating the structural stability of the nanowires under the cathodic CO reduction conditions (Figure S14).

The dependence of surface structures on the preparation conditions was corroborated by CO-TPD studies. The TPD patterns recorded for the Cu nanowires show CO desorption in a wide temperature range (i.e., 150−300 K), corresponding to CO binding energies varying from ∼40 to ∼80 kJ/mol (Figure 3b). Deconvolution of these patterns on the basis of the previously reported desorption temperatures for various single-crystal facets[24] (as well as the calculated CO binding energies, see the discussion below) gives four peaks associated with the four types of surface structures as observed in the voltammograms, namely, (111) at ∼180 K, (100) at ∼205 K, (110) at ∼230 K, and (211)* at ∼260 K. Although quantitative analysis of the TPD patterns may be obscured by the varying surface roughness factors, an explicit difference in surface structures can still be seen among the different types of Cu nanowires from the integrated peak areas. For example, the HR-150 nanowires have a substantially larger fraction (14.3%) of (110) facet exposed on the surface than the HR-300 (15 h) nanowires (3%, see Figure S15), whereas a reversed scenery was observed for the (211)* feature for these two types of nanowires (Figure 3c). The differences for the (111) and (100) facets are rather marginal. These observations are consistent with the findings from the electrochemical OH_{ad} studies.

We have performed DFT calculations to better understand the surface characterization results. Among the four types of

DOI: 10.1021/acscatal.7b01124
ACS Catal. 2017, 7, 4467−4472

facets considered here, Cu(110) has the highest surface energy, followed by (211), (100), and (111) (Figure 4a). Our calculations suggest that the relatively high-energy Cu(110) surface may be created by the removal of oxygen from the relatively low-energy (011) surface of CuO (see the Supporting Information for more details). The Cu(110) surface is likely metastable, as it does not show up on a calculated Wulff construction of the equilibrium shape for Cu nanocrystals,[25] which may explain the smaller fractions of (110) facet observed on the surface of Cu nanowires prepared at higher temperatures. It is also possible that the (110) surface undergoes a missing-row reconstruction upon annealing, as the reconstructed surface is calculated to have slightly lower surface energy (Figure 4a).[26,27] The calculated CO binding energies exhibit the trend (111) < (100) < (110) < (211) (Figure 4b), in support of the above assignment of CO desorption peaks in the TPD studies.

The OH_{ad} and CO-TPD results suggest that Cu(110) facets may be responsible for the high activity and selectivity of the HR-150 nanowires as compared to those prepared at higher temperatures. To understand the potential role of this open facet in the CO reduction electrocatalysis, we have used DFT calculations to elucidate the reaction pathways of CO reduction on the various Cu facets. Two possible mechanisms of C−C coupling, which is believed to be the rate-limiting step in CO reduction to produce C_2 species, are considered: one via the coupling of two *CHO to form *OCH−CHO*[28] and the other involving the direct coupling of *CO to form C_2 species.[15,16] The calculated onset potentials are the least negative potentials at which all reaction steps become exergonic, which are estimates of the upper (i.e., least negative) bounds of the real onset potentials do not include possible transition states for which the uncertainty in the calculated free energies may be high (see more details of the calculations in the Supporting Information). From the calculated free-energy diagrams, the upper bounds of the electrochemical potentials required for the CHO−CHO coupling mechanism are estimated to be −0.48, −0.36, −0.43, −0.45, and −0.57 V for the (211), (110), (110)-reconstructed, (100) and (111) surfaces, respectively (Figure 4c). The calculated potentials are consistent with experimental values on (100) and (111),[5,14] but the values are somewhat less negative than the previously reported theoretical values.[29−31] This could be due to the inclusion of van der Waals interactions in our calculations for hydrogenated adsorbates, which has been shown to provide more accurate adsorption energies for organic molecules.[32−35] A similar trend was found for the CO−CO coupling pathway to generate *COCHO or *COCOH, with upper bounds of −0.68, −0.34, −0.49, −0.31, and −0.53 V for the (211), (110), (110)-reconstructed, (100), and (111) surfaces, respectively (Figure 4d). If the reaction proceeds through an Eley−Rideal mechanism (Figure 4d), the calculated upper bounds of the onset potentials are −0.53, −0.14, −0.37, −0.20, and −0.53 V for the five types of surfaces. It is possible that on surfaces with high adsorption energy of OH, such as the (211) facet (Table S10), the adsorbed OH may limit CO reduction at low overpotentials.[23,30,36] These results indicate that Cu(110), having an intermediate binding strength to CO among the five facets studied here, may be the most active for the selective reduction of CO to C_2 species.

■ ASSOCIATED CONTENT

Supporting Information

The Supporting Information is available free of charge on the ACS Publications website at DOI: 10.1021/acscatal.7b01124.

Experimental methods and supplemental results as mentioned in the text (PDF)

■ AUTHOR INFORMATION

Corresponding Authors

*E-mail: tmueller@jhu.edu.
*E-mail: chaowang@jhu.edu.

ORCID

Kit H. Bowen: 0000-0002-2858-6352
Chao Wang: 0000-0001-7398-2090

Author Contributions

[¶]D.R. and L.C. contributed equally.

Notes

The authors declare no competing financial interest.

■ ACKNOWLEDGMENTS

This work was supported by the National Science Foundation (CHE-1437396). C.W. and D.R. also acknowledge support by the E[2]SHI Seed Grant and Catalyst Award from Johns Hopkins University. T.M. and L.C. acknowledge computational resources provided by XSEDE through award DMR-140068 and by the Maryland Advanced Research Computing Center (MARCC). Atomic-scale structural images were generated using VESTA.[37] This study made use of the Johns Hopkins University Department of Chemistry Core Facilities with Dr. Joel A. Tang's assistance. The authors also thank Mr. Robert Clapper from Shimadzu for the help on the GC-MS analysis. Participation of P. Rottmann and K. Hemker was supported by DOE Basic Energy Sciences (DE-FG02-07ER46437). X.T., Z.H., and K.B. acknowledge support by The Air Force Office of Scientific research (AFOSR) under Grant No. FA9550-15-1-0259 (KHB).

■ REFERENCES

(1) Hindermann, J. P.; Hutchings, G. J.; Kiennemann, A. *Catal. Rev.: Sci. Eng.* **1993**, *35*, 1−127.
(2) Gupta, M.; Smith, M. L.; Spivey, J. J. *ACS Catal.* **2011**, *1*, 641−656.
(3) Hori, Y.; Murata, A.; Takahashi, R.; Suzuki, S. *J. Am. Chem. Soc.* **1987**, *109*, 5022−5023.
(4) Schouten, K. J. P.; Kwon, Y.; van der Ham, C. J. M.; Qin, Z.; Koper, M. T. M. *Chem. Sci.* **2011**, *2*, 1902−1909.
(5) Schouten, K. J. P.; Qin, Z. S.; Gallent, E. P.; Koper, M. T. M. *J. Am. Chem. Soc.* **2012**, *134*, 9864−9867.
(6) Li, C. W.; Ciston, J.; Kanan, M. W. *Nature* **2014**, *508*, 504−507.
(7) Whipple, D. T.; Kenis, P. J. A. *J. Phys. Chem. Lett.* **2010**, *1*, 3451−3458.
(8) Olah, G. A.; Prakash, G. K. S.; Goeppert, A. *J. Am. Chem. Soc.* **2011**, *133*, 12881−12898.
(9) Singh, M. R.; Clark, E. L.; Bell, A. T. *Proc. Natl. Acad. Sci. U. S. A.* **2015**, *112*, E6111−E6118.
(10) Hori, Y. *Modern Aspects of Electrochemistry, No 42* **2008**, *42*, 89−189.
(11) Hori, Y.; Murata, A.; Yoshinami, Y. *J. Chem. Soc., Faraday Trans.* **1991**, *87*, 125−128.
(12) Hori, Y.; Takahashi, R.; Yoshinami, Y.; Murata, A. *J. Phys. Chem. B* **1997**, *101*, 7075−7081.
(13) Hori, Y.; Wakebe, H.; Tsukamoto, T.; Koga, O. *Surf. Sci.* **1995**, *335*, 258−263.

DOI: 10.1021/acscatal.7b01124
ACS Catal. 2017, 7, 4467−4472

(14) Schouten, K. J. P.; Perez Gallent, E. P.; Koper, M. T. M. *ACS Catal.* **2013**, *3*, 1292−1295.
(15) Calle-Vallejo, F.; Koper, M. T. M. *Angew. Chem., Int. Ed.* **2013**, *52*, 7282−7285.
(16) Montoya, J. H.; Shi, C.; Chan, K.; Norskov, J. K. *J. Phys. Chem. Lett.* **2015**, *6*, 2032−2037.
(17) Verdaguer-Casadevall, A.; Li, C. W.; Johansson, T. P.; Scott, S. B.; McKeown, J. T.; Kumar, M.; Stephens, I. E. L.; Kanan, M. W.; Chorkendorff, I. *J. Am. Chem. Soc.* **2015**, *137*, 9808−9811.
(18) Raciti, D.; Livi, K. J.; Wang, C. *Nano Lett.* **2015**, *15*, 6829−6835.
(19) Kohn, W.; Sham, L. J. *Phys. Rev.* **1965**, *140*, A1133−A1138.
(20) Feng, X.; Jiang, K.; Fan, S.; Kanan, M. W. *ACS Cent. Sci.* **2016**, *2*, 169−174.
(21) Wei, Y. J.; Anand, L. *J. Mech. Phys. Solids* **2004**, *52*, 2587−2616.
(22) Cantwell, P. R.; Tang, M.; Dillon, S. J.; Luo, J.; Rohrer, G. S.; Harmer, M. P. *Acta Mater.* **2014**, *62*, 1−48.
(23) Droog, J. M. M.; Schlenter, B. *J. Electroanal. Chem. Interfacial Electrochem.* **1980**, *112*, 387−390.
(24) Vollmer, S.; Witte, G.; Woll, C. *Catal. Lett.* **2001**, *77*, 97−101.
(25) Tran, R.; Xu, Z.; Radhakrishnan, B.; Winston, D.; Sun, W.; Persson, K. A.; Ong, S. P. *Sci. Data* **2016**, *3*, 160080.
(26) Spitzl, R.; Niehus, H.; Poelsema, B.; Comsa, G. *Surf. Sci.* **1990**, *239*, 243−253.
(27) Moritz, W.; Zuschke, R.; Pflanz, S.; Wever, J.; Wolf, D. *Surf. Sci.* **1992**, *272*, 94−101.
(28) Montoya, J. H.; Peterson, A. A.; Nørskov, J. K. *ChemCatChem* **2013**, *5*, 737−742.
(29) Durand, W. J.; Peterson, A. A.; Studt, F.; Abild-Pedersen, F.; Norskov, J. K. *Surf. Sci.* **2011**, *605*, 1354−1359.
(30) Peterson, A. A.; Abild-Pedersen, F.; Studt, F.; Rossmeisl, J.; Norskov, J. K. *Energy Environ. Sci.* **2010**, *3*, 1311−1315.
(31) Shi, C.; Chan, K.; Yoo, J. S.; Nørskov, J. K. *Org. Process Res. Dev.* **2016**, *20*, 1424−1430.
(32) Liu, W.; Savara, A.; Ren, X.; Ludwig, W.; Dostert, K.-H.; Schauermann, S.; Tkatchenko, A.; Freund, H.-J.; Scheffler, M. *J. Phys. Chem. Lett.* **2012**, *3*, 582−586.
(33) Liu, W.; Tkatchenko, A.; Scheffler, M. *Acc. Chem. Res.* **2014**, *47*, 3369−3377.
(34) Błoński, P.; López, N. *J. Phys. Chem. C* **2012**, *116*, 15484−15492.
(35) Sakong, S.; Groß, A. *ACS Catal.* **2016**, *6*, 5575−5586.
(36) Peterson, A. P.; Norskov, J. K. *J. Phys. Chem. Lett.* **2012**, *3*, 251−258.
(37) Momma, K.; Izumi, F. *J. Appl. Crystallogr.* **2008**, *41*, 653−658.

DOI: 10.1021/acscatal.7b01124
ACS Catal. 2017, 7, 4467−4472